Simulation Standard

TCAD Driven CAD

A Journal for Circuit Simulation and SPICE Modeling Engineers

RF CMOS Device Modeling : BSIM-Based Physical Model with Root-Like Construction Approach - Small Signal Modeling -

Ickjin Kwon, Minkyu Je, Kwyro Lee, and Hyungcheol Shin

Department of Electrical Engineering, Korea Advanced Institute of Science and Technology

Abstract

A novel extraction method of high frequency small-signal model parameters for MOSFET is proposed. From S-parameter measurement, this technique accurately extracts the MOSFET model parameters including the charge conservation capacitance parameters. To consider charge conservation, nonreciprocal capacitance is considered. The modeled S-parameters fit the measured ones well without any optimization after parameter extraction.

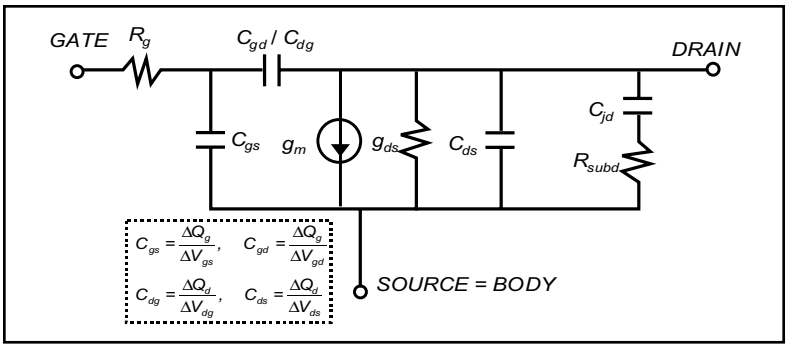

Figure 1. The proposed common-source equivalent circuit of a MOSFET after de-embedding parasitics of on-wafer pads and interconnection lines. Four independent intrinsic capacitances *Cgs, Cgd, Cdg,* and *Cds* are needed for charge conservation. The definitions of each capacitance are also shown.

I. Introduction

As the gate-length of MOSFET reduces, its high frequency characteristics improve [1][2]. MOSFET is good candidate for RF IC application because of low cost, high integration and one-chip solution possibility for analog and digital circuits. The extraction of small-signal equivalent circuit parameters is important for the development of accurate large signal model. Recently, many suggestions have been made to improve the prediction of AC properties at high frequencies. Simple modifications to the conventional MOSFET equivalent circuit and a few methods of extracting small-signal equivalent circuit parameters have been reported [3]-[5]. However these are based on the MESFET model and require complex curve fitting and optimization. They also do not consider charge conservation capacitance parameters which are important in intrinsic capacitance modeling. Previous small-signal equivalent circuit models that do not consider charge conservation cannot accurately model the intrinsic capacitance.

BSIM3v3 model has been recognized as an accurate and scalable Si MOSFET model at the low frequency range, however the parameter extraction procedure for high frequencies has not been established yet. In particular, submicron MOSFET capacitances are difficult to extract in the MHz frequency rangne and the numerical optimization process may fail to obtain the physical parameter. The determination of the model capacitances, based on large area C-V test structure measurement proved to be inaccurate in the high frequency range [8].

Continued on page 2....

INSIDE

SILVACO INTERNATIONAL

In this paper, we have developed a systematic parameter extraction method for MOSFET which includes charge conservation capacitance parameters, from measured S-parameters, and verified the results match well with measured data.

II. New Extraction Method of Small-Signal Parameters

The proposed common-source equivalent circuit of a MOSFET after de-embedding parasitics of on-wafer pads and interconnection lines is shown in Figure 1. The circuit elements between the substrate and source are excluded because the substrate is short-circuited to the source as in most high-frequency application. In this case, the substrate resistance that exists between the source and substrate is negligible. The proposed equivalent circuit is basically scalable since all its element are physically meaningful. The gate resistance Rg represents the effective channel resistance which consists of the distributed channel resistance seen from the gate and the distributed gate electrode resistance [9], which affect the input admittance Y11 at RF. The drain junction capacitance and the bulk spreading resistance are represented by Cjd and Rsubd. Substrate coupling effects through the drain junction and the substrate resistance play an important role for the output admittance Y_{22} [6].

In the source-body tied three terminal structure, four independent intrinsic capacitances *Cgs*, *Cgd*, *Cdg*, and *Cds* are needed for charge conservation. The definitions of each capacitance are shown in Figure 1. The gate current *Ig* and the drain current *Id* and their associated charges *Qg* and *Qd* are related by the following equations.

$$i_g = \frac{dQ_g}{dt} = \frac{fQ_g}{fV_{gs}}\frac{dV_{gs}}{dt} + \frac{fQ_g}{fV_{gd}}\frac{dV_{gd}}{dt} = C_{gs}\frac{dV_{gs}}{dt} + C_{gd}\frac{dV_{gd}}{dt} \quad (1)$$

$$i_d = \frac{dQ_d}{dt} = \frac{fQ_d}{fV_{dg}}\frac{dV_{dg}}{dt} + \frac{fQ_d}{fV_{ds}}\frac{dV_{ds}}{dt} \quad (2)$$

We have written Cdg and Cgd separately in the above equations, and Cdg is not equal to Cgd because of the difference in the signal excitation direction. These non-reciprocal capacitances are necessary for charge conservation of small signal model [10]. In equivalent circuit of MOSFET shown in Figure 1, overlap capacitances are included in Cgs, Cgd, Cdg and intrinsic capacitances are obtained by de-embedding overlap capacitances. The new extraction procedure uses linear regression approach for the Y-parameters which are converted from measured S-parameters. The small-signal equivalent circuit shown in Figure 1 can be analyzed in terms of Y-parameters as follows,

$$Y_{11} = \frac{\omega^2 (C_{gs}+C_{gd})^2 R_g + j\omega(C_{gs}+C_{gd})}{1+\omega^2 (C_{gs}+C_{gd})^2 R_g{}^2} \quad (3)$$

$$Y_{12} = \frac{-\omega^2 C_{gd}(C_{gs}+C_{gd})^2 R_g - j\ _{gd}}{1+\omega^2 (C_{gs}+C_{gd})^2 R_g{}^2} \quad (4)$$

$$Y_{21} = \frac{g_m - \omega^2 C_{dg}(C_{gs}+C_{dg})^2 R_g - j\omega C_{dg} - j\omega g_m R_g (C_{gs}+C_{dg})}{1+\omega^2 (C_{gs}+C_{dg})^2 R_g{}^2} \quad (5)$$

$$Y_{22} = g_{ds} + \frac{\omega^2 C_{jd}{}^2 R_{subd} + j\omega C_{jd}}{1+\omega^2 C_{jd}{}^2 R_{subd}{}^2} + j\omega C_{ds} + \frac{\omega^2 C_{dg}{}^2 R_g + j\omega C_{dg} + j\omega^3 R_g{}^2 C_{gs} C_{dg}(C_{gs}+C_{dg})}{1+\omega^2 (C_{gs}+C_{dg})^2 R_g{}^2} \quad (6)$$

For operation frequencies up to 10GHz, $\omega^2(C_{gs}+C_{gd})^2 Rg^2 << 1$, $\omega^2(C_{gs}+C_{gd})^2 R_g{}^2 << 1$, and $<< 1$. By using these assumptions, Y-parameters can be expressed as following.

$$Y_{11} \cup \omega^2 (C_{gs}+C_{gd})^2 R_g + j\omega(C_{gs}+C_{gd}) \quad (7)$$

$$Y_{12} \cup -\omega^2 C_{gd}(C_{gs}+C_{gd}) R_g - j\omega C_{gd} \quad (8)$$

$$Y_{21} \cup g_m - \omega^2 C_{dg}(C_{gs}+C_{dg})^2 R_g - j\omega C_{dg} - j\omega g_m R_g (C_{gs}+C_{dg}) \quad (9)$$

$$Y_{22} \cup g_{ds} + \frac{\omega^2 C_{jd}{}^2 R_{subd}}{1+\omega^2 C_{jd}{}^2 R_{subd}{}^2} + \omega^2 C_{dg}{}^2 R_g + \frac{j\omega C_{jd}}{1+\omega^2 C_{jd}{}^2 R_{subd}{}^2} + j\omega C_{ds} + j\omega C_{dg} \quad (10)$$

Parameter extraction is performed from real and imaginary parts of the above Y-parameters. Cg_d, Rg, C_{gs}, g_m, C_{dg}, and g_{ds} can be obtained by Eq. (11)-(16). g_m and g_{ds} are obtained from y-intercept of $Re[Y_{21}]$ versus ω^2 and from intercept of $\mathrm{Re}[Y_{22}]$ versus ω^2, respectively.

$$C_{gd} = -\mathrm{Im}[Y_{12}]/\omega \quad (11)$$

$$R_g = \mathrm{Re}[Y_{11}]/(\mathrm{Im}[Y_{11}])^2 \quad (12)$$

$$C_{gs} = \mathrm{Im}[Y_{11}]/\omega - C_{gd} \quad (13)$$

$$g_m = \mathrm{Re}[Y_{21}]\Big|_{\omega^2=0} \quad (14)$$

$$C_{dg} = \frac{-\mathrm{Im}[Y_{21}]/\omega - g_m R_g C_{gs}}{1+g_m R_g} \quad (15)$$

$$g_{ds} = \mathrm{Re}[Y_{22}]\Big|_{\omega^2=0} \quad (16)$$

R_{subd} and C_{jd} are obtained from linear regression of $\omega^2 / [Re[Y_{22}] - g_{ds} - \omega^2 C_{dg}^2 R_g]$ vs. ω^2 using the following relation.

$$\frac{\omega^2}{\mathrm{Re}[Y_{22}] - g_{ds} - \omega^2 C_{dg}^{\ 2} R_g} = \omega^2 R_{subd} + \frac{1}{C_{jd}^{\ 2} R_{subd}} \qquad (17)$$

Rs_{ubd} is determined from slope of $\omega^2/[Re[Y_{22}] - g_{ds} - \omega^2 C_{dg}^2 R_g]$ as a function of ω^2 and C_{jd} is extracted from (18).

$$C_{ds} = \mathrm{Im}[Y_{22}]/\omega - C_{dg} - \frac{C_{jd}}{1 + \omega^2 C_{jd}^{\ 2} R_{subd}^{\ 2}} \qquad (19)$$

Finally, C_{ds} is obtained from (19) as

III. Parameter Extraction Results

The test devices are multi-fingered n-MOSFET's of AMS 0.35 µm CMOS technologies having unit gate width of 5 µm. The parameter extraction has been performed for an n-MOSFET with 100 mm width having twenty-unit gate fingers. To remove pad parasitics, de-embedding technique was carried out by subtracting parasitics of open pad structure from measured device S-parameters.

The small signal parameters including charge conservation capacitance parameters were extracted at V_{gs} = 1 V and V_{ds} = 2 V using Eq. (11)-(19). Transconductance g_m of 16.6 mS was obtained from y-intercept of Re[Y_{21}] versus ω^2 as shown in Figure 2(a) and conductance g_{ds} of 0.31 mS was obtained from intercept of Re[Y_{22}] versus ω^2, as shown in Figure 2(b). R_{subd} of 200 Ω was determined from slope of $\omega^2 / [\mathrm{Re}[Y_{22}] - g_{ds} - \omega^2 C_{dg}^2 R_g]$ as a function of ω^2 as shown in Figure 3.

The frequency dependence of extracted small-signal capacitance parameters for the n-MOSFET biased to V_{gs} = 1 V and V_{ds} = 2 V are shown in Figure 4. Also, extracted gate resistance R_g as a function of frequency for the n-MOSFET biased to V_{gs} = 1 V and V_{ds} = 2V is shown in Figure 5. The frequency range is from 0.5 GHz to 10.5 GHz. The results shows that extracted parameters remains almost constant with frequency. Figure 4 and Figure 5 verified that this extraction method is accurate and reliable.

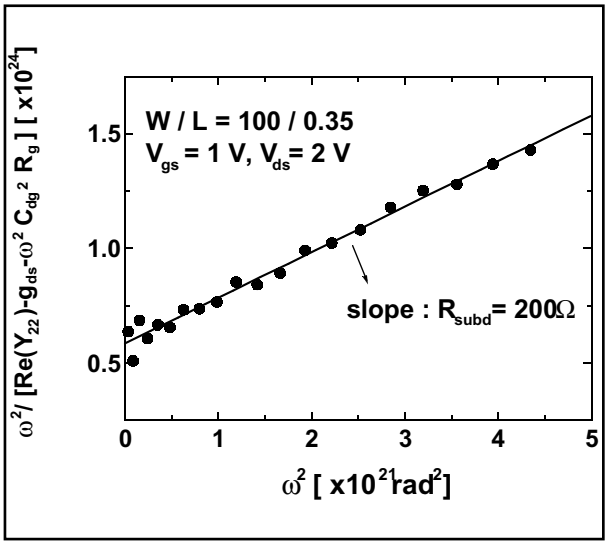

Fig. 3. Rsubd was determined from the slope of w2 / [Re[Y22] - gds - w2Cdg2Rg] as a function of w2. Extracted value of Rsubd was 200 W.

For the extracted parameter values, $\omega^2 (C_{gs} + C_{gd})^2 R_g^{\ 2}$ is calculated to be 0.06 at 10 GHz, which is much smaller than one. This verifies the validity of using the assumption in simplifying Eq. (3) – Eq. (6) to Eq. (7) – Eq. (10).

Figure 6 shows measured and modeled Y-parameters using extracted model parameters and the small signal equivalent circuit shown in Figure 1. It shows that the modeled S-parameter fit the measured ones well without any optimization after parameter extraction.

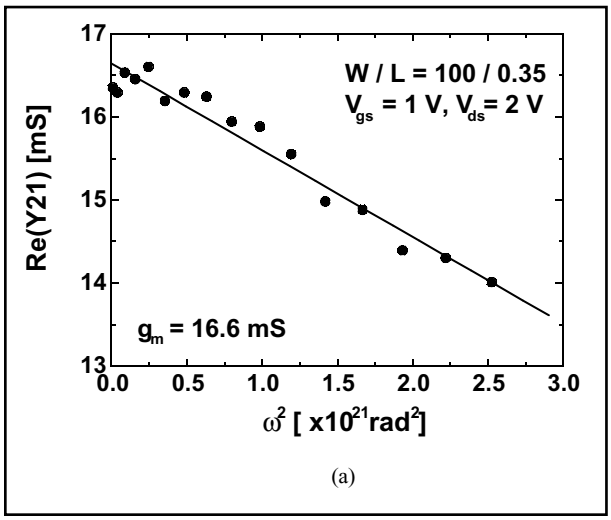

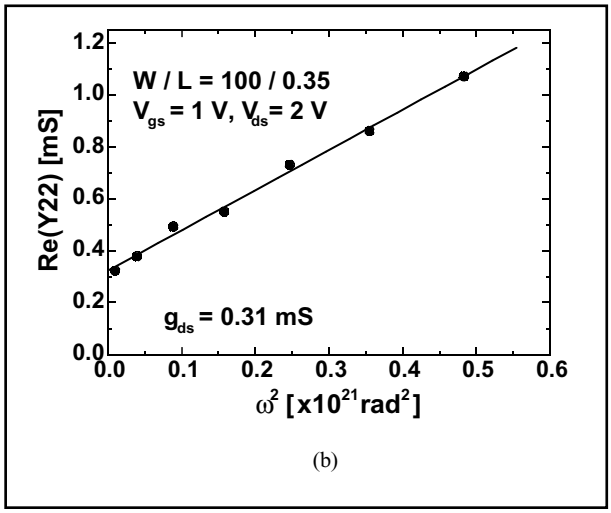

Fig. 2. Extraction of conductance gm and gds. (a) gm was obtained from y-intercept of Re[Y21] versus w2 . Extracted value of gm was 16.6 mS. (b) gds was obtained from y-intercept of Re[Y22] versus w2 . Extracted value of gds was 0.31 mS.

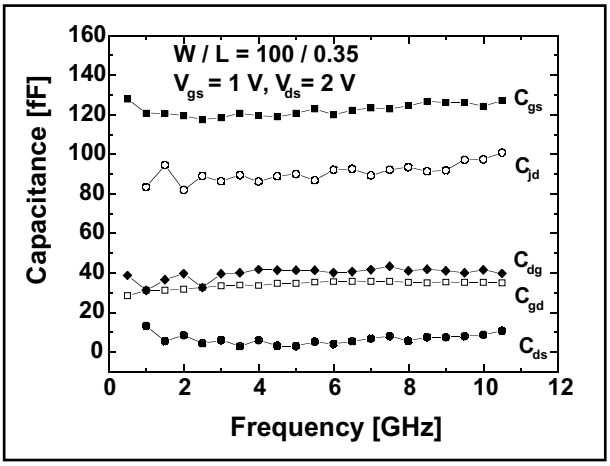

Figure 4. The frequency dependence of extracted capacitance parameters for an n-MOSFET having 100 mm width and biased to Vgs = 1 V and Vds = 2 V. Extracted parameters remain almost constant with frequency.

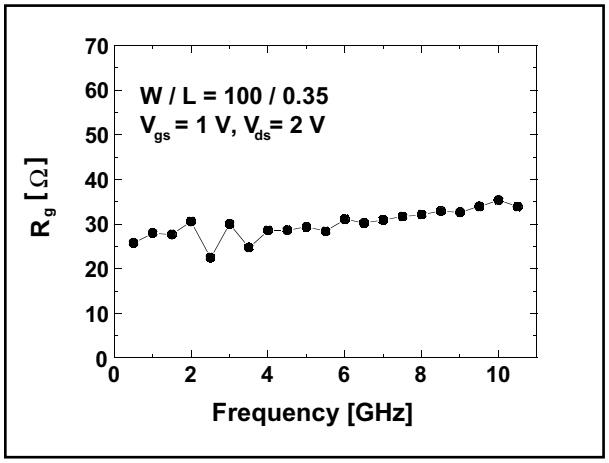

Figure 5. The frequency dependence of gate resistance Rg for an n-MOSFET having 100 mm width and biased to Vgs = 1 V and Vds = 2 V. Gate resistance Rg remains almost constant with frequency.

The admittance Y_{11} fits the measured data well with gate resistance model and Y_{22} fits well with substrate resistance model. The non-reciprocal capacitance C_{gd} and C_{dg} contribute to match imaginary part of Y_{12} and Y_{21}.

In Figure 7, gate-bias dependence of the extracted small-signal parameters for the n-MOSFET biased to Vds = 2 V is shown. In Fig. 7(a), Cgs increases gradually as gate bias increases in the saturation region and drops in the linear region. Since the intrinsic gate-drain capac-

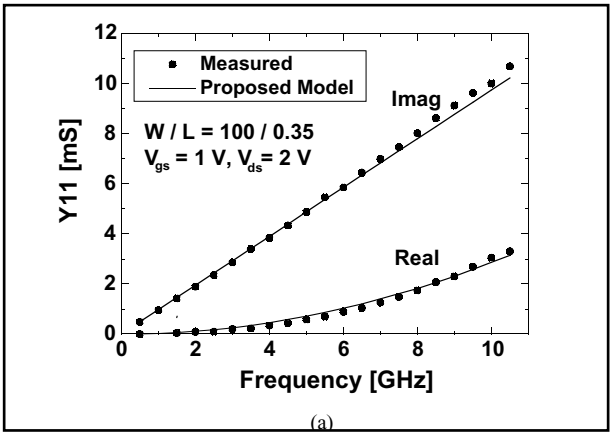

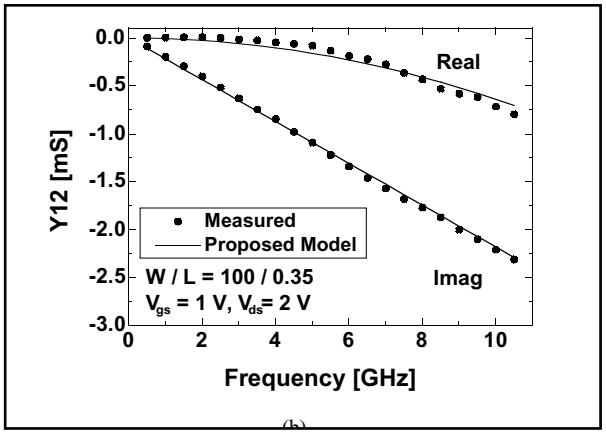

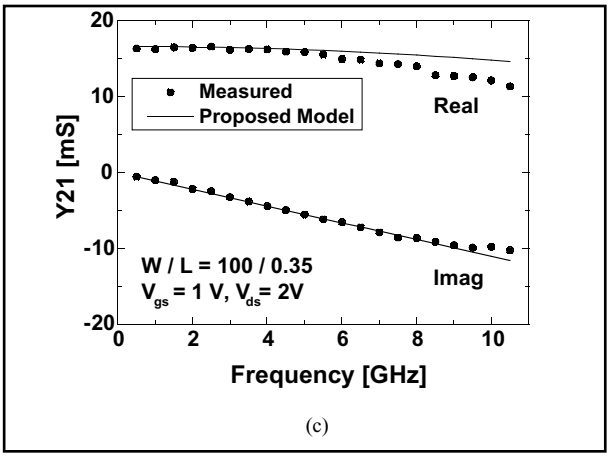

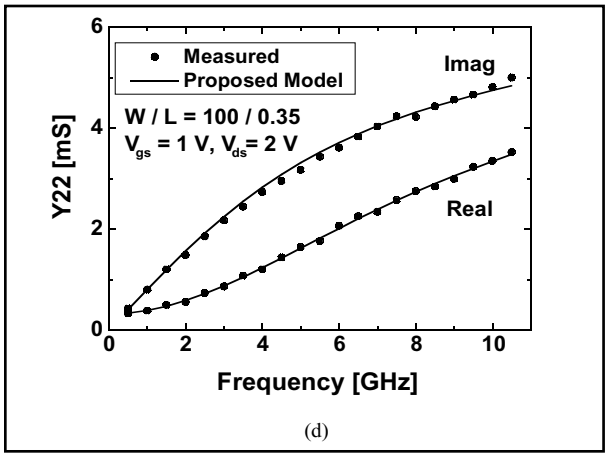

Figure 6. The measured and modeled Y-parameters using extracted model parameters for the n-MOSFET biased to Vgs = 1 V and Vds = 2 V. The frequency range is from 0.5 GHz to 10.5 GHz. (a)Y11 (b)Y12 (c)Y21 (d)Y22. It shows that the modeled S-parameters fit the measured ones well without any optimization after parameter extraction.

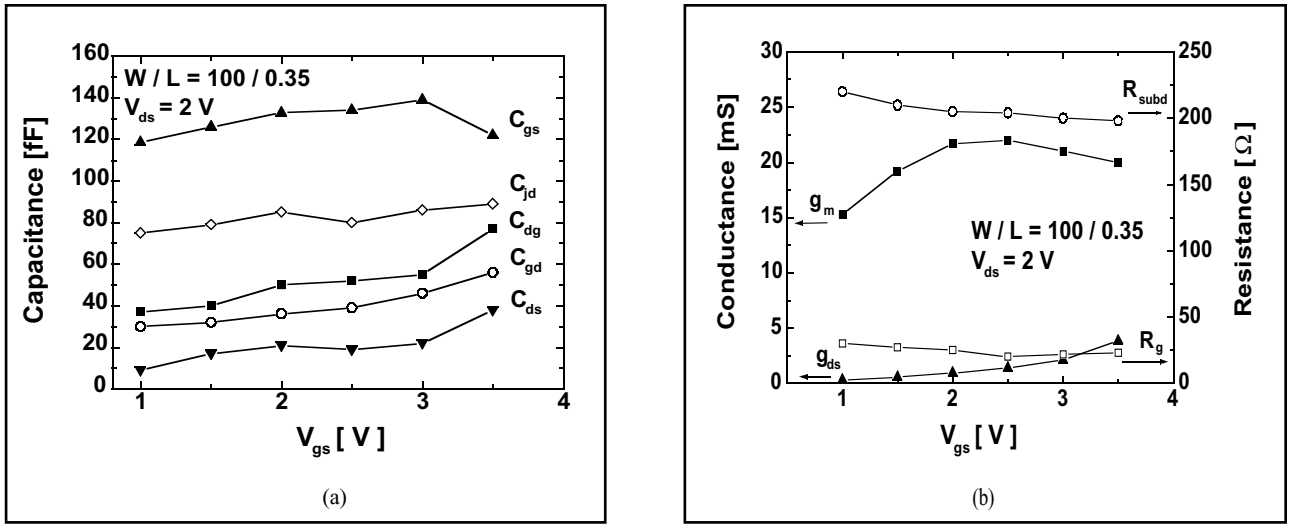

Fig. 7. The gate-bias dependence of extracted parameters for an n-MOSFET having 100 mm width and biased to Vds = 2 V. (a) Capacitances (b) Conductances and resistances.

itance is small compared to overlap capacitance in the saturation region, Cgd and Cdg are almost constant in the saturation region and increase gradually in the linear region. The smooth behaviors for Cgs, Cgd and Cdg are because the region-to-region transition is very gradual due to short-channel effects. Fig. 7(b) shows that transconductance gm increases as gate bias increases for small Vgs and gm decreases for high gate bias due to mobility degradation. Drain conductance gds increases almost proportional to gate bias in the saturation region due to short channel effects and gds rapidly increases with Vgs in the linear region because for higher gate bias drain current increases more rapidly with drain bias in the linear region.

IV. Conclusions

A novel extraction method of obtaining an accurate high frequency small-signal parameters for MOSFET has been demonstrated. The nonreciprocal capacitance was introduced and this technique accurately extracted the charge conservation capacitance parameters. The proposed model from parameter extraction has been evaluated with measured S-parameter and good agreement has been observed. Developed extraction method is an effective parameter extraction technique for the large-signal BSIM3v3 model.

References

[1] C. Wann, L. Su, K. Jenkins, R. Chang, D. Frank, Y. Taur, "RF Perspective of Sub-Tenth-Micron CMOS," IEEE International Solid-State Circuits Conference, pp. 254-255, 1998.

[2] E. Morifuji, et al., Future perspective and scaling down roadmap for RF CMOS, Symposium on VLSI Technology Digest of Technical Papers, pp. 163-164, 1999.

[3] D. Lovelace, J. Costa, N. Camilleri, "Extracting Small-Signal Model Parameters of Silicon MOSFET Transistors", IEEE MTT-S Digest, 1994, pp.865-868.

[4] G. D. Dambrine, A. Cappy, F. Helidore, and E. Palyze, "A new method for determining the FET small-signal equivalent circuit." IEEE Trans. Microwave Theory Tech., vol. 36, pp. 173-176, 1998.

[5] S. Lee, H. K. Yu, C. S. Kim, J. G. Koo, and K. S. Nam, "A novel approach to extracting small-signal model parameters of silicon MOSFET's," IEEE Microwave and guided wave letters, vol. 7, pp. 75-77, 1997.

[6] W. Liu, R. Gharpurey, M. C. Chang, U. Erdogan, R. Aggarwal, and J. P. Mattia, "RF MOSFET modeling accounting for distributed substrate and channel resistance with emphasis on the BSIM3v3 SPICE model," in IEDM Tech. Dig., pp.309-312, Dec. 1997.

[7] J. J. Ou, X. Jin, I. Ma, C. Hu, "CMOS RF modeling for GHz communication IC's," VLSI Symp. On Tech., Dig. of Tech. Papers, pp. 94-95, June 1998.

[8] D. R. Pehlke, M. Schroder, A. Burstein, M. Matloubian, M. F. Chang, "High frequency application of MOS compact model and their development for scalable RF model libraries," Proc. of CICC, pp. 219-222, May 1998.

[9] X. Jin, J. J. Ou, C-H C, W. Liu, J. Deen, P. R. Gray, C. Hu, "An Effective Gate Resistance Model for CMOS RF and Noise modeling," in IEDM Tech. Dig., 1998.

[10] Ping Yang, Berton D. Epler, Pallab K. Chatterjee, "An Investigation of the Charge conservation Problem for MOSFET Circuit Simulation", IEEE Journal of Solid-State Circuits, vol. Sc-18, no. 1. Feb, 1983.

VBIC Version 1.2 Released in *SmartSpice* and *UTMOST III*

Introduction

The latest VBIC bipolar model v1.2 of Sep 24 1999 has been integrated into ***SmartSpice*** and ***UTMOST III***. It can be invoked by specifying the model selector LEVEL=5 and the version selector VERSION=1.2. in the .MODEL card. This new version becomes the default VBIC model.

A new model parameter REVISION has been introduced to invoke future updates or older VBIC models. In ***SmartSpice/UTMOST III***, only the old version 1.1.5 is still supported and can be invoked by specifying VERSION=1.1 and REVISION=5. If other values are given, v1.2 is assumed. Aliases are listed in Table 1.

The explicit specification of VERSION and REVISION is strongly recommended to avoid incompatibility problems between v1.1.5 and v1.2.

New Features in VBIC v1.2:

Here is a summary list of major updates and enhancements announced in v1.2 and relative to v1.1.5:

- temperature dependence of IKF,
- separate temperature coefficients for intrinsic and extrinsic resistances RCX, RBX and RBP,
- simple exponential base-emitter breakdown model,
- reach-through model to limit base-collector depletion capacitances,
- separate activation energy for ISP,
- selector available to switch to SGP qb formulation,
- high-current roll-off coefficient,
- fixed collector-substrate capacitance,
- separate IS allowed for reverse operation in HBTs,
- error fixed in the built-in potential temperature mapping (psibi function).

All these new features have been implemented in ***SmartSpice***. Only the 3-terminal version of the model described in the official release is not currently supported. Due to some of these changes, VBICv1.2 is not fully backward compatible with the previous version (1.1.5).

New Model Parameters in VBICv1.2:

All parameters supported in v1.1.5 are still used in v1.2. However, the definition has slightly changed for the following ones:

Due to the separation of the temperature dependence for intrinsic and extrinsic resistances, XRC and XRB now correspond to XRCI and XRBI, respectively. Aliases XRCI and XRBI have been added for convenience.

Due to changes in the formulation of the single piece depletion capacitance model, the smoothing factors AJE, AJC, AJS are now expressed in volts.

VBICv1.2 has 19 new model parameters that are shown in Table 2.

New Temperature Mappings

The following abbreviations are defined for convenience:

where *TNOM* is the temperature at which model parameter extraction has been done. T_d corre-sponds to the dynamic temperature if self-heating is turned on or to the operating temperature otherwise.

- A bug in psibi mapping with temperature has been

$$V_{td} = \frac{k \cdot T_d}{q},\ V_{tnom} = \frac{k \cdot TNOM}{q} \text{ and } r_{td} = \frac{T_d}{TNOM}$$

  fixed. The psibi function is used to calculate built-in potentials PE, PC and PS at the device temperature as a function of related model parameters and activation energies EAIE, EAIC and EAIS, respectively. The updated expressions are (actually, only the expression *pssio* has been corrected):

$$psiio(P) = 2.0 \cdot V_{tnom} \cdot \log\left(\exp\left(\frac{P}{2.0 \cdot V_{tnom}}\right) - \exp\left(-\frac{P}{2.0 \cdot V_{tnom}}\right)\right)$$

$$psiin(P, Ea, T_d) = psiio \cdot r_{td} - 3.0 \cdot V_{td} \cdot \log(r_{td}) - Ea \cdot (r_{td} - 1.0)$$

$$psibi(P, Ea, T_d) = psiin + 2.0 \cdot V_{td} \cdot \log\left[\left(1.0 + \sqrt{1.0 + 4.0 \cdot \exp\left(-\frac{psiin}{V_{td}}\right)}\right) / 2.0\right]$$

Parameter (alias)	Description	Units	Default
VERSION (VERS)	Version parameter. Only 1.1 (if REV=5) and 1.2 (if REV= 0) are permitted, otherwise 1.2 is assumed.	-	1.2
REVISION (REV, VREV)	Revision parameter. Only 0 (if VERS=1.2) and 5 (if VERS=1.1) are permitted, otherwise 0 is assumed.	-	0

Table 1.

Parameter (alias)	Description	Units	Default
XRBX	Temperature exponent of extrinsic resistance RBX	-	0.0
XRCX	Temperature exponent of extrinsic resistance RCX	-	0.0
XRBP	Temperature exponent of extrinsic resistance RBP	-	0.0
XIKF	Temperature exponent of IKF	-	0.0
ISRR	Reverse saturation current factor (HBTs)	-	1.0
XISR	Temperature exponent of ISRR (HBTs)	-	0.0
DEAR	Activation energy shift for ISRR (HBTs)	V	0.0
EAP	Activation energy for ISP	V	1.12
VBBE	Base-Emitter breakdown voltage, zero means infinity	V	0.0
TVBBE1	First temperature coefficient of VBBE		0.0
TVBBE2	Second temperature coefficient of VBBE		0.0
NBBE	Base-Emitter breakdown emission coefficient	-	1.0
TNBBE	Temperature coefficient of NBBE		0.0
IBBE	Base-Emitter breakdown current	A	1.0e-6
QBM	Selector for SGP qb formulation	-	0.0
NKF	High current roll-off coefficient	-	0.5
VRT	B-C reach-through limiting voltage (0 means infinity)	V	0.0
ART	B-C reach-through limiting smoothing factor	V	0.1
CCSO	Fixed collector-substrate capacitance	F	0.0

Table 2.

- Some equations have been updated according to new model parameters:

$$RCX(T_d) = RCX \cdot (r_{td})^{XRCX}$$ (new paramerter XRCX)

$$RBX(T_d) = RBX \cdot (r_{td})^{XRBX}$$ (new paramerter XRBX)

$$RBP(T_d) = RBP \cdot (r_{td})^{XRBP}$$ (new paramerter XRBP)

$$ISP(T_d) = ISP \cdot (r_{td})^{\frac{XIS}{NFP}} \cdot \exp\left(-\frac{EAP}{NFP} \cdot \frac{1.0 - r_{td}}{V_{td}}\right)$$ (new paramerter EAP)

- New equations have been added:

$$IKF(T_d) = IKF \cdot (r_{td})^{XIKF}$$ (new parameter XIKF)

$$ISRR(T_d) = ISRR \cdot (r_{td})^{\frac{XISR}{NR}} \cdot \exp\left(-\frac{DEAR}{NR} \cdot \frac{1.0 - r_{td}}{V_{td}}\right)$$ (new parameters ISSR, XISR, DEAR)

$$VBBE(T_d) = VBBE \cdot (1.0 + TVBBE1 \cdot (T_d - TNOM) + TVBBE2 \cdot (T_d - TNOM)^2)$$ (new parameters ISSR, XISR, DEAR)

$$NBBE(T_d) = NBBE \cdot (1.0 + TNBBE \cdot (T_d - TNOM))$$ (new parameters VBBE, TVBBE1, TVBBE2)

$$EBBE(T_d) = \exp\left(-\frac{VBBE(T_d)}{NBBE(T_d) \cdot V_{td}}\right)$$

New Current Equations

- The equation of the ideal reverse current has been modified to account for a separate saturation current IS in reverse operation (HBTs). However backward compatibility is maintained if new model parameters ISSR, XISR and DEAR are unspecified (default values lead to). The new equation is:

$$Itri = IS(T_d) \cdot ISSR(T_d) \cdot \left(\exp\left(\frac{Vbci}{NR \cdot Vtd}\right) - 1.0\right)$$

- Two expressions for the base charge equation are now available and can be selected using the model parameter QBM. The standard Gummel-Poon formulation has been introduced. The high-current roll-off coefficient NKF is also supported. If NKF is unspecified, its default value is equal to 0.5 and the first expression reduces to $qb = 0.5 \cdot q1 + \sqrt{q1^2 + 4 \cdot q2}$ for back-ward compatibility with v1.1.5.

if (QBM<0.5)(default)

$$qb = 0.5 \cdot \left[q1 + \left(q1^{\frac{1}{NKF}} + 4 \cdot q2\right)^{NKF}\right]$$

else

$$qb = 0.5 \cdot q1 \cdot (1.0 + (1.0 + 4 \cdot q2)^{NKF})$$

- If VBBE > 0.0, a new contribution is added to intrinsic and extrinsic base-emitter currents Ibe and Ibex to account for the B-E breakdown effect:

$$Ibei = IBEI \cdot \left(\exp\left(\frac{Vbei}{NEI \cdot Vtd}\right) - 1.0\right)$$

$$Iben = IBEN \cdot \left(\exp\left(\frac{Vbei}{NEN \cdot Vtd}\right) - 1.0\right)$$

$$Ibebk = IBEE \cdot \left(\exp\left(\frac{-VBBE(T_d) - Vbei}{NBBE(T_d) \cdot Vtd}\right) - EBBE(T_d)\right)$$

$$Ibe = WBE \cdot [Ibei + Iben - Ibebk]$$

$$Ibexi = IBEI \cdot \left(\exp\left(\frac{Vbex}{NEI \cdot Vtd}\right) - 1.0\right)$$

$$Ibexn = IBEN \cdot \left(\exp\left(\frac{Vbex}{NEN \cdot Vtd}\right) - 1.0\right)$$

$$Ibexbk = IBEE \cdot \left(\exp\left(\frac{-VBBE(T_d) - Vbex}{NBBE(T_d) \cdot Vtd}\right) - EBBE(T_d)\right)$$

$$Ibex = (1.0 - WBE) \cdot [Ibexi + Ibexn - Ibexbk]$$

New Charge Equations

- A new depletion capacitance model with optional reach-through limiting has been introduced to evaluate normalized depletion charges qdbc and qdbep (other depletion charges are still evaluated using the function qj). Assuming that V is the junction applied voltage, P is the junction built-in potential, FC is the forward bias depletion capacitance limit, M is the junc-tion grading coefficient and AJ is the smoothing factor, the new function qjrt is defined by:

If $AJ \le 0$

Define $dvh = V - FC \cdot P$

If $dvh > 0.0$ (large forward bias)

$$qj = P \cdot \frac{1.0 - (1.0 - FC)^{1.0-M}}{1.0 - M} + dvh \cdot \frac{1.0 - FC + \frac{dvh \cdot M}{2.0 \cdot P}}{(1.0 - FC)^{1.0+M}}$$

else if $VRT > 0.0$ and $V < -VRT$ (new equation for large reverse bias)

$$qj = \frac{P}{1.0 - M} \cdot \left(1.0 - \left(1.0 + \frac{VRT}{P}\right)^{1.0-M} \cdot \left[1.0 - \frac{(1.0 - M) \cdot (V + VRT)}{(P + VRT)}\right]\right)$$

(NEW)

else (medium forward and reverse bias)

$$qj = P \cdot \frac{1.0 - \left(1.0 - \frac{V}{P}\right)^{1.0-M}}{1.0 - M}$$

else (single piece model)

If $VRT > 0.0$ and $ART > 0.0$ (new parameters VRT and ART)

Define $dv0 = -FC \cdot P$

$$vn0 = \frac{VRT + dv0}{VRT - dv0}$$

$$vnl0 = \frac{2 \cdot vn0}{\sqrt{(vn0 - 1.0)^2 + 4 \cdot AJ^2} + \sqrt{(vn0 + 1.0)^2 + 4 \cdot ART^2}}$$

$$l0 = 0.5 \cdot (vnl0 \cdot (VRT - dv0) - VRT - dv0)$$

$$qlo0 = P \cdot \frac{1.0 - \left(1.0 - \frac{vl0}{P}\right)^{1.0-M}}{1.0 - M}$$

$$vn = \frac{2.0 \cdot V + VRT + dv0}{VRT - dv0}$$

$$vnl = \frac{2 \cdot vn}{\sqrt{(vn - 1.0)^2 + 4 \cdot AJ^2} + \sqrt{(vn + 1.0)^2 + 4 \cdot ART^2}}$$

$$vl = 0.5 \cdot (vnl \cdot (VRT - dv0) - VRT - dv0)$$

$$qlo = P \cdot \frac{1.0 - \left(1.0 - \frac{vl}{P}\right)^{1.0-M}}{1.0 - M}$$

$$sel = 0.5 \cdot (vnl + 1.0)$$

$$crt = \left(1.0 + \frac{VRT}{P}\right)^{-M}$$

$$cmx = (1.0 - FC)^{-M}$$

$$cl = (1.0 - sel) \cdot crt + sel \cdot cmx$$

$$ql = (V - vl + vl0) \cdot cl$$

$$qjrt = ql + qlo - qlo0$$

else (no reach-through limiting)

$$vl = 0.5 \cdot \left(V - FC \cdot P - \sqrt{(V - FC \cdot P)^2 + 4 \cdot AJ^2}\right) + FC \cdot P$$

$$vl0 = 0.5 \cdot \left(-FC \cdot P - \sqrt{(-FC \cdot P)^2 + 4 \cdot AJ^2}\right) + FC \cdot P$$

$$qj = -P \cdot \frac{\left(1.0 - \frac{vl}{P}\right)^{1.0-M}}{1.0 - M} + \frac{V - vl + vl0}{(1.0 - FC)^M} + P \cdot \frac{\left(1.0 - \frac{vl0}{P}\right)^{1.0-M}}{1.0 - M}$$

It is important to notice that qj and qjrt functions are identical if VRT is set to zero (no reach- through limiting). The influence of the reach-through limiting on normalized depletion capacitances only occurs for reverse biased junction as shown on Figure 1 and Figure 2. Figure 1 corresponds to the SGP-like model, where the depletion capacitance linearly increases for values of forward bias greater than FC.P. Figure 2 corresponds to the single piece model where the depletion capacitance smootly limits to its value at FC.P. The effect of reach-through limiting is similar for both models.

Continued on page 11....

Calendar of Events

January

1 New Years Day
2
3
4
5
6
7
8
9
10
11
12
13
14
15
16
17
18
19
20
21
22
23
24
25
26
27 EDA TechnoFair, Yokohama, Japan
28 EDA TechnoFair, Yokohama, Japan
29
30
31

February

1
2
3
4
5
6
7
8
9
10
11
12
13
14
15
16
17
18
19
20
21
22
23
24
25
26
27
28
29

Bulletin Board

EDA Techofair

The premier EDA tradeshow in Japan will be anchored once again by the presence of Silvaco International. With major staffing from our Japan office and corporate headquarters in the U.S., plus nine workstations to demonstrate our tools, be prepared to understand why we are the emerging EDA leader.

10 Years of Publication

Simulation Standard has just completed its tenth year of publication! Since 1990, Silvaco has delivered this valuable tool to our constituents. The first issue debuted under the title "The Exterminator" in May 1990. In June 1992, Simulation Standard was sent out for the first time. Currently, our newsletter reaches tens of thousands of designers worldwide. Thank you for making it a success!

Another Record Tradeshow Year

The year 2000 will set another record for tradeshow exhibitions by Silvaco. After meeting many of you at our thirty-three tradeshows in 1999, we are embarking on an aggressive schedule of over forty shows for 2000. To execute this task, Silvaco has handed the tradeshow torch from David Warren to Mr. Ryan Melius as the new Tradeshow Marketing Manager.

For more information on any of our workshops, please check our web site at ***http://www.silvaco.com***

Hints, Tips and Solutions

Mustafa Taner, Applications and Support Engineer

Q. How can I characterize the parasitic BJT behavior of SOI devices using *UTMOST III*.

A. ***UTMOST III*** SOI module has three routines for characterization of the parasitic BJTs of SOI devices. These routines are "IC/VCE", "Gummel" and "INT_BJT" All routines require to have 5 terminal devices with bulk connection for data collection.

The "Gummel" routine sweeps the voltage for the bulk terminal and keeps a constant voltage for the gate, source, drain and backgate terminals. The measured currents are drain and bulk currents. However during this measurement the bulk and drain diodes can be on and the diode current can be added to the bulk current. This additional diode current prevents the user from characterizing the pure intrinsic bipolar device.

The "INT_BJT" routine was developed to exclude any additional diode currents which may contribute to the intrinsic bipolar behavior. In order to achieve this goal the source terminal bias was swept and bulk and drain terminals were kept at the same potential (typically at ground potential). The gate potential's effect on the parasitic bipolar behavior was also investigated. Therefore the VGS bias stepping function was added to the routine (Figure 1). In order to keep the VGS bias constant the VG bias has to follow the sweeping bias of VS. The constant VGS bias is obtained by using the "offset" (VAR1') function of the DC analyzers HP4145 and HP4155/56. The HP4142 DC analyzer uses the point by point (user mode) measurement technique to keep the constant VGS bias.

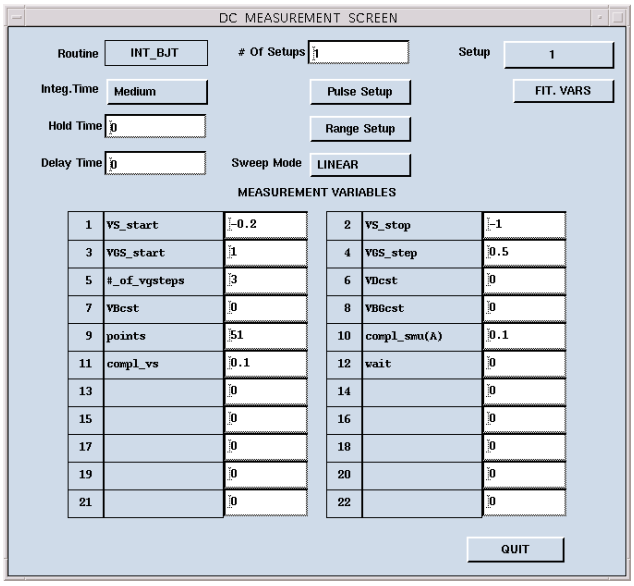

Figure 1. The Set measureemnt screen of the INT_BJT routine.

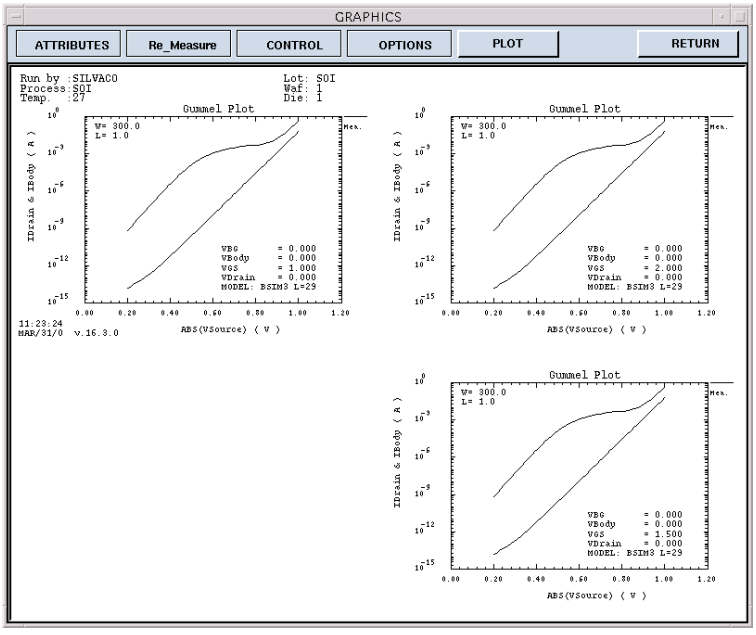

Figure 2. Idrain and Ibulk currents versus VSB voltage at three different VGS bias points.

The "INT_BJT" routine displays the measured drain and bulk currents versus VSB (source to bulk) voltage (Figure 2). The global and local optimization techniques can be utilized to extract parameters which are used to model the parasitic bipolar behavior in SOI devices. The important model parameters of the parasitic bipolar device in BSIM3v3 partially depleted SOI model are:

ISBJT (BJT injection saturation current)

NBJT (Power coefficient of channel length dependency for bipolar current)

LBJT0 (Reference channel length for bipolar current)

VABJT (Early voltage for bipolar current)

AELY (Channel length dependency of early voltage for bipolar current)

AHLI (High level injection parameter for bipolar current)

Q. Can Silvaco provide a bipolar modeling service using the advanced bipolar models such as MEXTRAM and VBIC?

A. Yes. Both MEXTRAM and VBIC models have been implemented in ***SmartSpice*** and ***UTMOST III***. Silvaco characterization lab provides the advanced bipolar modeling service using both models as well as Gummel-Poon and Macro models.

The advanced bipolar models provide many advantages over the Gummel-Poon and Macro models. Some of the major advantages can be listed as:

- Improved early effect modeling
- Quasi-saturation modeling. (Both Gummel Poon (including level=2 GP model) and macro models can not model this behavior)
- Parasitic substrate current modeling. (The Gummel-Poon is three terminal model and it doesn't include the substrate node. The Macro models can handle the substrate current but the modeling of the parasitic devices of the Macro model are not accurate)
- Avalanche multiplication modeling.

Call for Questions

If you have hints, tips, solutions or questions to contribute, please contact our Applications and Support Department

Phone: (408) 567-1000 Fax: (408) 496-6080

e-mail: *support@silvaco.com*

Hints, Tips and Solutions Archive

Check our our Web Page to see more details of this example plus an archive of previous Hints, Tips, and Solutions

www.silvaco.com

...continued from page 8

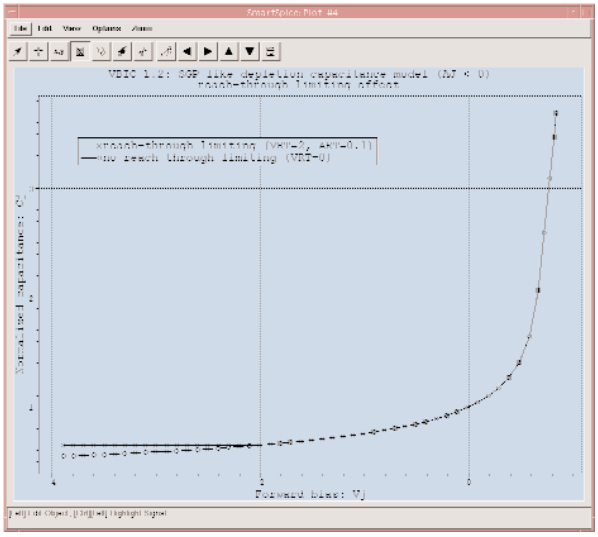

Figure 1.

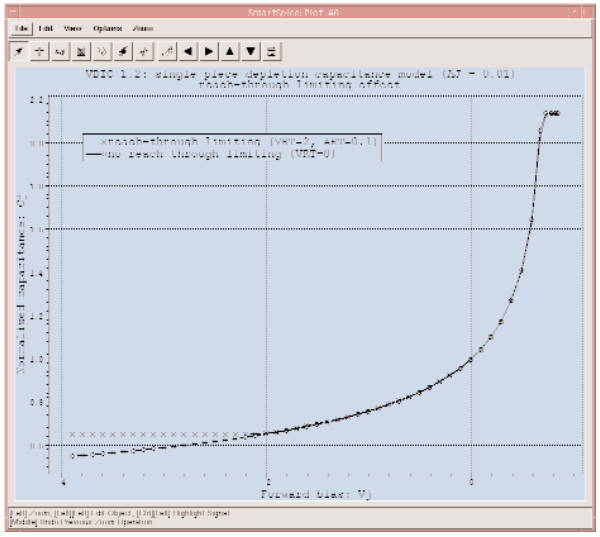

Figure 2.

Another important point is that the qj function implemented in v1.1.5 has been slightly modified in v1.2. The smoothing factor AJ has been replaced by 4*AJ*AJ in vl and vl0 expressions.

- The contribution of the fixed capacitance CCSO has been added to the base-collector charge Qbcp of the parasitic device. The new equation is:

$$Qbcp = qdbcp \cdot CJCP(T_d) + CCSO \cdot Vbcp$$

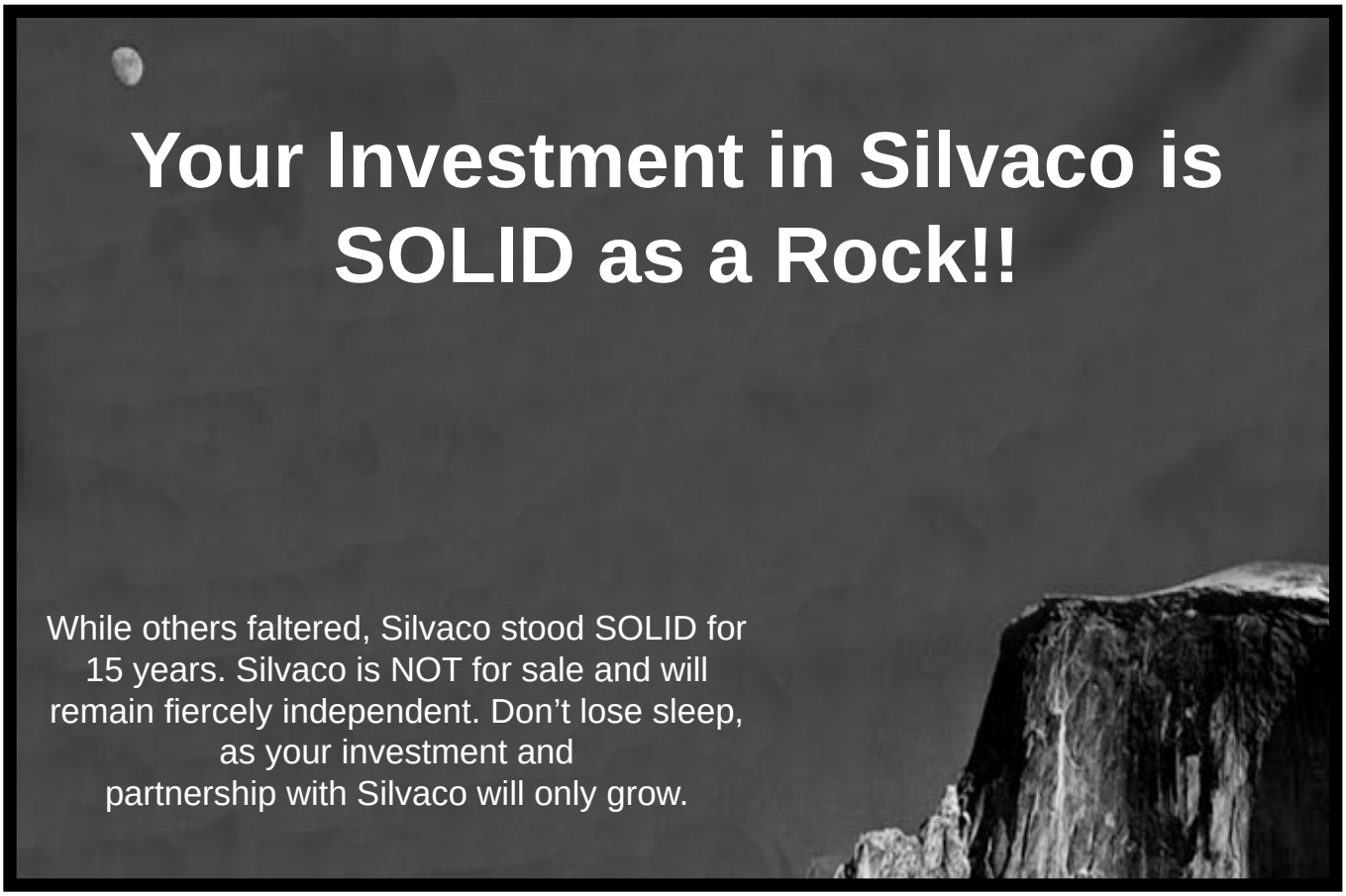

SILVACO
INTERNATIONAL

USA HEADQUARTERS

Silvaco International
4701 Patrick Henry Drive
Building 2
Santa Clara, CA 95054
USA

Phone: 408-567-1000
Fax: 408-496-6080

sales@silvaco.com
www.silvaco.com

CONTACTS:

Silvaco Japan
jpsales@silvaco.com

Silvaco Korea
krsales@silvaco.com

Silvaco Taiwan
twsales@silvaco.com

Silvaco Singapore
sgsales@silvaco.com

Silvaco UK
uksales@silvaco.com

Silvaco France
frsales@silvaco.com

Silvaco Germany
desales@silvaco.com

Products Licensed through Silvaco or e*ECAD

e*ECAD
Vendor Partner